

# Vector field path following and obstacle avoidance singularity mitigation via look-ahead flight envelope

First A. Author\* and Second B. Author Jr.†  
*Business or Academic Affiliation 1, City, State, Zip Code*

**Unmanned Aerial Vehicles conventionally navigate by following a series of pre-planned waypoints that may have to be re-planned when flying in a dynamic environment or encountering previously unknown obstacles. Waypoints are generally planned off-line and relayed to the UAV, taking up time and autopilot communication resources. Attractive path following and repulsive obstacle avoidance vector fields have been summed together to produce UAV guidance that follows pre-planned paths and avoids obstacles without the need to re-plan. Summing attractive and repulsive vector fields may produce small regions of null guidance, called singularities, which could potentially lead to trap situations. An investigation into singularity mitigation by vector field weight parameterization is presented.**

## I. Nomenclature

*UAV* = Unmanned Aerial Vehicle  
*VF* = Vector Field  
*VFF* = Virtual Force Field  
*LVF* = Lyapunov Vector Field  
*GVF* = Goncalves Vector Field

## II. Introduction

Unmanned Aerial Vehicles (UAV)s are pilotless aircraft used by military, police, and civilian communities for tasks such as reconnaissance, damage assessment, surveying, and target tracking [1, 2]. Tasks can be performed by a single UAV or cooperate with a team of other air, ground, or marine vehicles [3–5]. UAVs are ideal for remote data collection due to their low cost, endurance, and reduced risk to human life. Data can be collected by loitering the aircraft around an area of interest (AOI) or along a sensor path, such as a road or tree-line. Missions for collecting data are typically pre-planned on a remote ground station where an obstacle free and flyable path is generated. Constraints such as optimizing sensor converge may be considered when planning [6]. Typically paths are deconstructed into a series of discrete waypoints that the UAV navigates to through the use of a line-of-sight guidance. While navigating the pre-planned path previously unknown obstacles may be discovered and a new obstacle free path may have to be generated, which may be difficult or impossible if the UAV is out of radio range. Additional methods for avoiding obstacles in real time include potential field and vector field which employ the use of artificial attractive and repulsive forces to pull a UAV towards a goal while pushing away from obstacles. Potential field is a popular solution to both path planning and guidance problems in obstacle rich environments, however suffers from several limitations including local minima, oscillations, and may cause excess deviation from the desired sensor line. Vector field guidance converges and circulates a pre-defined path and may be summed with additional repulsive vector fields to produce an obstacle avoidance. Further optimization of vector field produces a real-time guidance for avoiding obstacles and returning to a pre-planned sensor path with minimal deviation. Obstacle avoidance using waypoint guidance, potential field, and vector field will be discussed. Each method will be compared in simulation for both deviation from the sensor path and for cross track error with respect to the geometric optimal avoidance path. The optimized vector field will then be demonstrated on a crazyflie 2.0 multi-rotor simulating fixed wing constraints.

---

\*Insert Job Title, Department Name, Address/Mail Stop, and AIAA Member Grade (if any) for first author.

†Insert Job Title, Department Name, Address/Mail Stop, and AIAA Member Grade (if any) for second author.

### A. Waypoint Navigation

UAVs missions are traditionally accomplished by following a series of waypoints that lie on a off-line and pre-planned path. Many methods can be used for generating paths, however the process is generally executed in two steps consisting of optimization and refinement. Optimization builds shortest path taking in constraints such as obstacles and mission objectives. For surveying or mapping missions the objective is to maximize the time spent over a given sensor line or path to provide sensors with the opportunity to collect valuable data. If an obstacle lies along that sensor path, the UAV must avoid the obstacle but also return back to the sensor path such that a minimal length of the path is missed during data collection. A geometrically optimal path around a circular obstacle for a vehicle with fixed turn rate constraints can be generated in three steps. First, the UAV turns away from the obstacle such that it eventually becomes tangent to the obstacle radius. The vehicle then would proceed to follow the outside of the obstacle until nearly approaching the original sensor path. The UAV would then turn back towards the intended sensor path. An example of a series of waypoints that route a UAV with fixed wing constraints around an obstacle is shown in Figure 1 below.

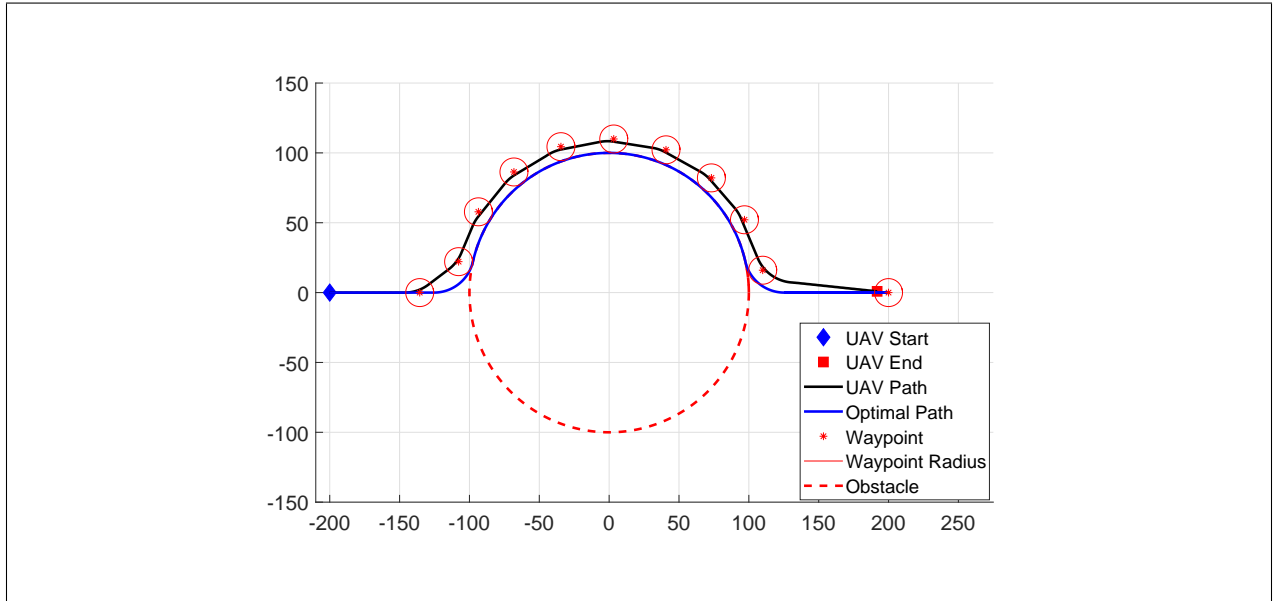


**Fig. 1 Simulated Fixed Wing UAV Traversing Waypoints Around Circular Obstacle**

During waypoint navigation the UAV may encounter obstacles or environmental changes that would require a new obstacle free series of waypoints to be generated. UAVs that rely on off-board path planning would relay the updated environment information to the ground where a new optimized, refined, and obstacle free path would be re-planned. Waypoints would be constructed along the updated path and relayed back to the UAV. For highly uncertain or dynamic environments, path planning may have to occur frequently which may be impossible if the UAV is flying beyond LOS or needs to maintain radio silence. In the event communication is possible, the latency of waypoint updates may not be frequent enough and the UAV may fail to avoid obstacles all together. Obstacle avoidance without re-planning can be accomplished with on-board guidance systems that direct the UAV around the obstacle and return to the path.

### B. Potential Field

Potential field has been used as a path planning, trajectory planning, and control method [8] for robotic systems in static and dynamic environments by applying a field of artificial attractive and repulsive forces [7]. Goals are represented as an attractive force that pulls a point mass in the direction of minimal energy. Obstacles are represented as repulsive forces that act locally to push a point mass away. The gradient of the potential can be used as a guidance vector to transit towards a goal while avoiding obstacles. Riding the gradient from an initial position to the goal results in a goal seeking and obstacle avoidance path.

An example of potential field can be found in [9–11] which allowed for real time goal seeking with obstacle avoidance on a mobile ground robot equipped with ultrasonic sensors. The robot located at  $(x_0, y_0)$  is attracted towards a goal with constant magnitude force  $\vec{F}_t$  located at  $(x_t, y_t)$  and a distance  $d_t$  from the robot. Obstacles are detected

within a pre-defined window containing a fixed number of cells. Cells containing an obstacle provide a repulsive force  $\vec{F}_{i,j}$  opposite in direction to the line-of-sight from vehicle to cell location  $(x_i, y_j)$ , where  $(i, j)$  represents the cell index,  $F_{cr}$  is a constant repulsive force,  $W$  the vehicle's width,  $C_{i,j}$  a cell's certainty, and  $d_{i,j}$  the distance to the center of the cell with respect to robots center.

$$\vec{F}_{i,j} = \frac{F_{cr} W^n C_{i,j}}{d_{i,j}^n} \left( \frac{x_i - x_0}{d_{i,j}} \hat{x} + \frac{y_i - y_0}{d_{i,j}} \hat{y} \right) \quad (1)$$

The total repulsive force exerted on the robot is determined by summing the active cells, shown in Equation 2

$$\vec{F}_r = \sum_{i,j} \vec{F}_{i,j} \quad (2)$$

$$\vec{F}_t = F_{ct} \left( \frac{x_t - x_0}{d_t} \hat{x} + \frac{y_t - y_0}{d_t} \hat{y} \right) \quad (3)$$

Summing together attractive and repulsive forces produce a vector that can be used for heading guidance, shown in Equation 4.

$$\vec{R} = \vec{F}_r + \vec{F}_t \quad (4)$$

Major drawbacks to potential field were identified in [11] consisting of local minimum and oscillations in corridors. The local minimum problem occurs when closely spaced obstacle's potential combine to produce a well on the descent gradient where a pre-mature stable point is reached. Proposed solutions to local minimum include object clustering and virtual waypoint method [12], virtual escaping route [13], and use of navigation functions [14]. Oscillations in potential field were studied in [15] and [16].

In addition to local minimum and oscillations, potential field may converge to a singular point which is not possible for fixed wing aircraft since it must maintain a minimum forward velocity to remain airborne. With a velocity constraint a vehicle would need to update the position of the goal point periodically as the UAV approaches the goal. Simulating a UAV using VFF for heading guidance for a Dubins vehicle was performed and is shown in Figure 2, where a single obstacle cell located at the origin. The UAV initially travels directly toward the goal located at (50, 0) until the obstacle is encountered, at which point a repulsive force is applied. The UAV avoids the obstacle, however significantly deviates and fails to get back on the path between waypoints. For certain applications it may be beneficial to follow explicit paths for tasks such as data collection on a roadway or searching a tree line.

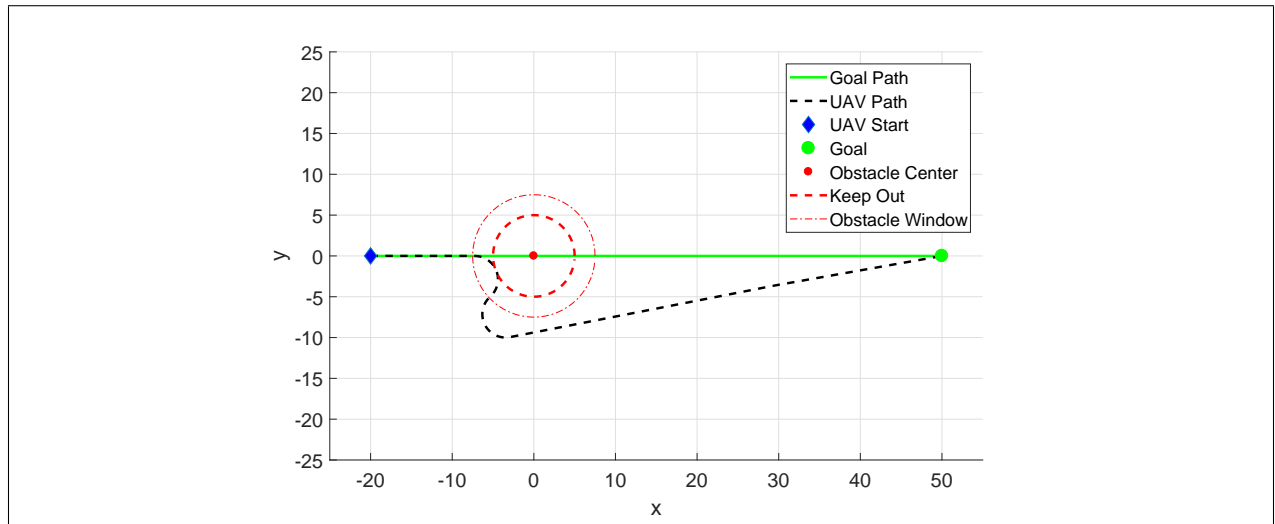


**Fig. 2 Dubins vehicle encountering an obstacle while navigating to a waypoint**

Following an explicit path to collect data or follow a ground target can be accomplished with vector fields, which produce a heading guidance that asymptotically converges and circulates a path. A comparison between vector field

and waypoint guidance techniques was presented in [17] where each method was evaluated based on its complexity, robustness, and accuracy. The vector field model produced guidance that was both robust to external wind disturbances while maintaining a low cross track error. The two most prominent methods for generating vector fields in literature consist of the Lyapunov [18–23] and Goncalves [24–27] method. Lyapunov vector fields for converging and following straight and circular paths were described in [18].

Straight and circular path vector fields can be selectively activated throughout flight to form more complex paths, shown in [18–20, 28]. Lyapunov vector field for curved path following was presented in [23] which may allow for more complex paths and eliminates the need to switch between vector fields.

### C. GVF

The Goncalves Vector Field (GVF) method produces a similar field, however has several advantages over LVFs. GVF produces an  $n$ -dimensional vector field that converges and circulates to both static and time varying paths. Additionally, convergence, circulation, and time-varying terms that make up the GVF are decoupled from each other allowing for easy weighting of the total field. GVFs converge and circulate at the intersection, or level set, of  $n - 1$  dimensional implicit surfaces ( $\alpha_i : \mathbb{R}^n \rightarrow \mathbb{R} | i = 1, \dots, n - 1$ ). The integral lines of the field are guaranteed to converge and circulate the level set when two conditions are met: 1) the implicit surface functions are positive definite and 2) have bounded derivatives.

The total vector field  $\vec{V}$  is calculated by:

$$\vec{V} = G\nabla V + H \wedge_{i=1}^{n-1} \nabla \alpha_i - LM(\alpha)^{-1}a(\alpha) \quad (5)$$

or in component form:

$$\vec{V} = G\vec{V}_{conv} + H\vec{V}_{circ} + L\vec{V}_{tv} \quad (6)$$

where  $\vec{V}_{conv}$  produces vectors perpendicular to the path,  $\vec{V}_{circ}$  produces vectors parallel to the path, and  $\vec{V}_{tv}$  is a feed-forward term that produces vectors accounting for a time varying path.

Convergence is calculated by:

$$\vec{V}_{conv} = \nabla V \quad (7)$$

where scalar  $G$  is multiplied by the gradient of the definite potential function  $V$ :

$$V = -\sqrt{\alpha_1^2 + \alpha_2^2} \quad (8)$$

$$\nabla V = \begin{bmatrix} \frac{dV}{dx} \\ \frac{dV}{dy} \\ \frac{dV}{dz} \end{bmatrix} \quad (9)$$

Circulation is calculated by taking the wedge product of the gradients of the surface functions:

$$\vec{V}_{circ} = \wedge_{i=1}^{n-1} \nabla \alpha_i \quad (10)$$

In the case of ( $n = 3$ ) the wedge product simplifies as the cross product:

$$\vec{V}_{circ} = \nabla \alpha_1 \times \nabla \alpha_2 \quad (11)$$

The feed-forward time-varying component is calculated by:

$$\vec{V}_{tv} = M^{-1}a \quad (12)$$

where,

$$M = \begin{bmatrix} \nabla \alpha_1^T \\ \nabla \alpha_2^T \\ (\nabla \alpha_1 \times \nabla \alpha_2)^T \end{bmatrix} \quad (13)$$

$$a = \left[ \frac{\partial \alpha_1}{\partial t} \quad \frac{\partial \alpha_2}{\partial t} \quad 0 \right]^T \quad (14)$$

Intersecting two flat planes ( $\alpha_1 = z, \alpha_2 = x$ ) produces a GVF that converges and circulates a straight path, shown in Figure 4.

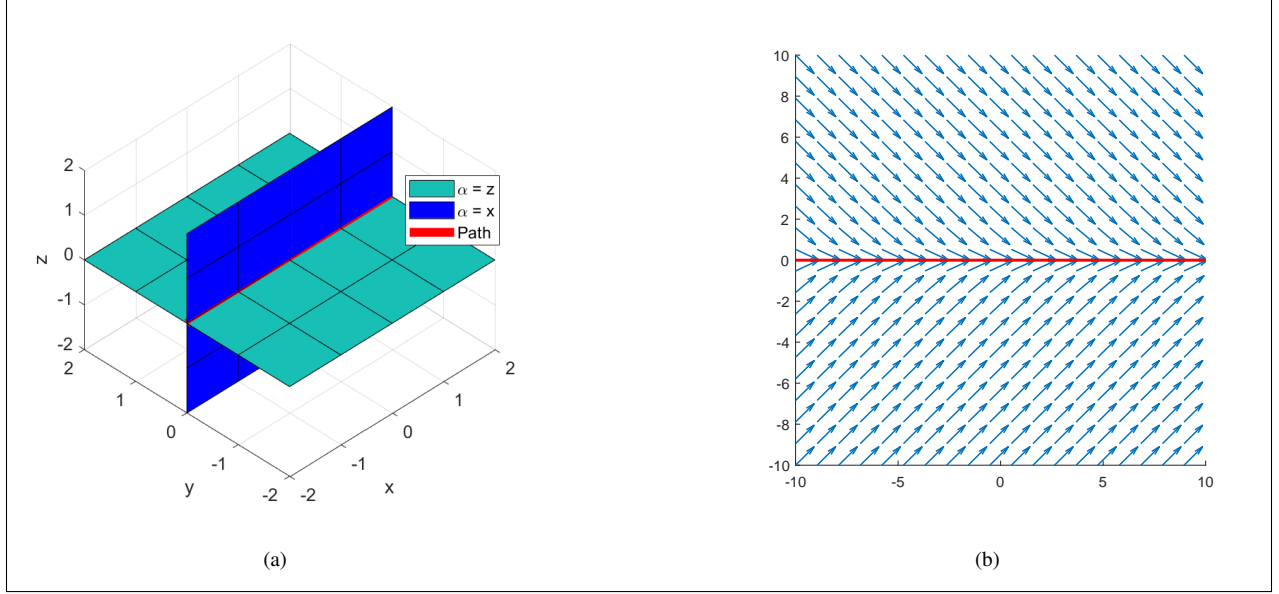


**Fig. 3 GVF converging and circulating straight path**

A GVF for converging and circulating a circular path can be produced by intersecting a plane and a cylinder ( $\alpha_1 = z, \alpha_2 = x^2 + y^2 - r^2$ ).

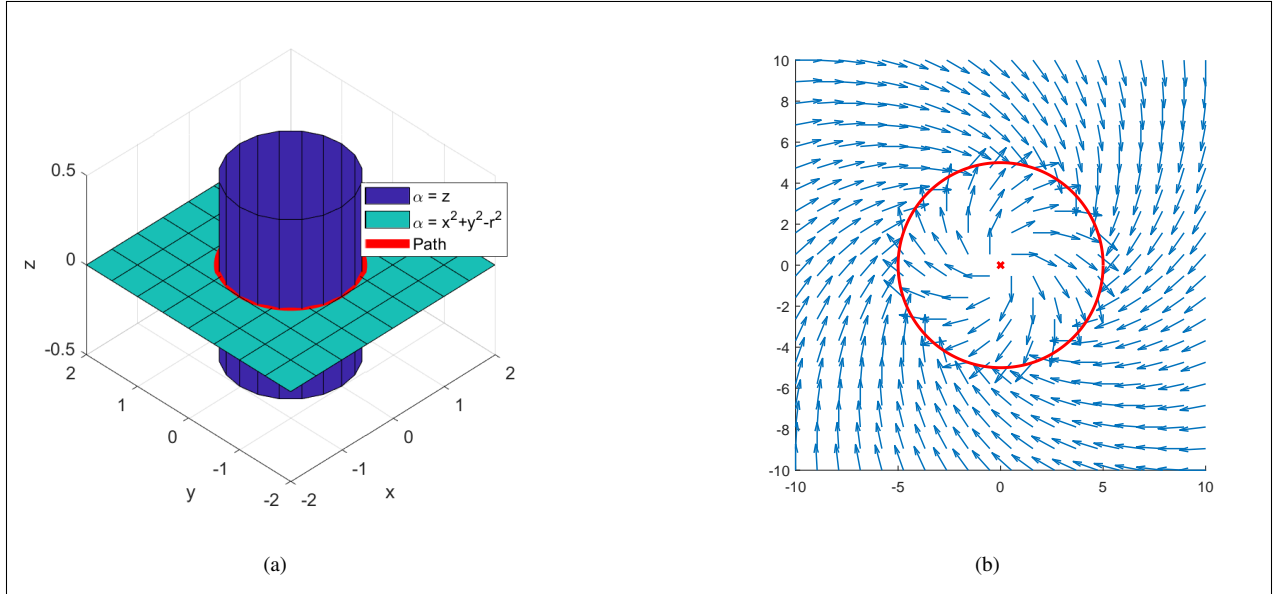


**Fig. 4 GVF converging and circulating circular path**

GVF was compared against LVP in a standoff tracking scenario in [Wilhelm] where a fixed wing UAV was tasked with with loitering around a moving ground target while avoiding static obstacles. A circular time-varying attractive vector field was attached to a moving ground target. Static circular repulsive vector fields centered at the obstacles

and weighted by hyperbolic tangent decay functions were summed with the attractive circular field to produce a target loitering and obstacle avoidance guidance. The performance of Lyapunov [21] and gradient vector field [24–26] were compared for their cross track error with respect to the loiter circle. Gradient vector field had favorable performance due to compensation for a time-varying vector field. The gradient vector field technique also has the benefit of decoupled weighting parameters for convergence, circulation, and time-varying terms, allowing for easy modification of field behavior.

Decay functions for avoidance fields using GVF were investigated in [Zhu] for obstacles present on a straight path. When summing attractive and repulsive vector fields there is the possibility of guidance singularities, where magnitude and direction are equal and opposite. The presence of singularities were not addressed in [Wilhelm] and [Zhu], mentioned briefly in [18] and observed in [29]. For fixed wing UAVs the lack of guidance may prevent the UAV from avoiding an obstacle, while multi-rotor UAVs may end up in a trap situation. Singularities may be present at any location where a goal field and obstacle field are of equal strength.

#### D. Dubins Vehicle

Dubin's vehicle's position  $\vec{X}$  at time  $t$  is calculated from the integral of the velocity vector  $\vec{U}$ . The vehicle has a constant velocity magnitude  $u_{uav}$  at a heading  $\theta$ . The rate at which  $\theta$  changes with respect to time is based on limitations of the craft itself.

$$\vec{U}(t) = u_{uav} \begin{bmatrix} \cos(\theta(t)) \\ \sin(\theta(t)) \end{bmatrix} \quad (15)$$

$$\vec{X}(t) = \vec{U} dt + \vec{X}(t-1) \quad (16)$$

$$\dot{\theta} \leq 20 \text{deg/s} \quad (17)$$

### III. methods

Overview of methods  
 Construction of guidance for desired path  
 Construction of avoidance guidance  
 Path following and obstacle avoidance guidance  
 Singularity detection  
 Selection of vf parameters for optimized obstacle avoidance

#### A. Path Following with GVF

Path following guidance for a planar UAV at position  $(x, y)$  for a time invariant line is achieved by summing together convergence  $\vec{V}_{conv}$  and circulation  $\vec{V}_{circ}$  terms shown in Equation ??.

where the plane defined by implicit surface function  $\alpha_1$  is at angle  $\delta$  and plane  $\alpha_2$  is at constant height of  $Z = 1$  shown in Equations 18 and 19 respectively.

$$\alpha_1 = \cos(\delta)x + \sin(\delta)y \quad (18)$$

$$\alpha_2 = z \quad (19)$$

The gradient  $\nabla$  of the potential function  $V$  is shown in Equation 20.

$$\nabla V = - \frac{1}{2(\sqrt{\cos^2(\delta)x^2 + 2\cos(\delta)\sin(\delta)xy + \sin^2(\delta)y^2})} \begin{bmatrix} 2x\cos^2(\delta) + 2\cos(\delta)\sin(\delta)y \\ 2y\sin^2(\delta) + 2\cos(\delta)\sin(\delta)x \\ 2 \end{bmatrix} \quad (20)$$

Circulation is calculated by the cross product of the surface function gradients, shown in Equation ?? and 21.

$$\vec{V}_{circ} = \begin{bmatrix} \sin(\theta) \\ -\cos(\theta) \\ 0 \end{bmatrix} \quad (21)$$

Guidance for a path at angle  $\delta = 0$  and equal parts circulation and convergence weights  $G = H = 1$  is shown in Figure 5 below.

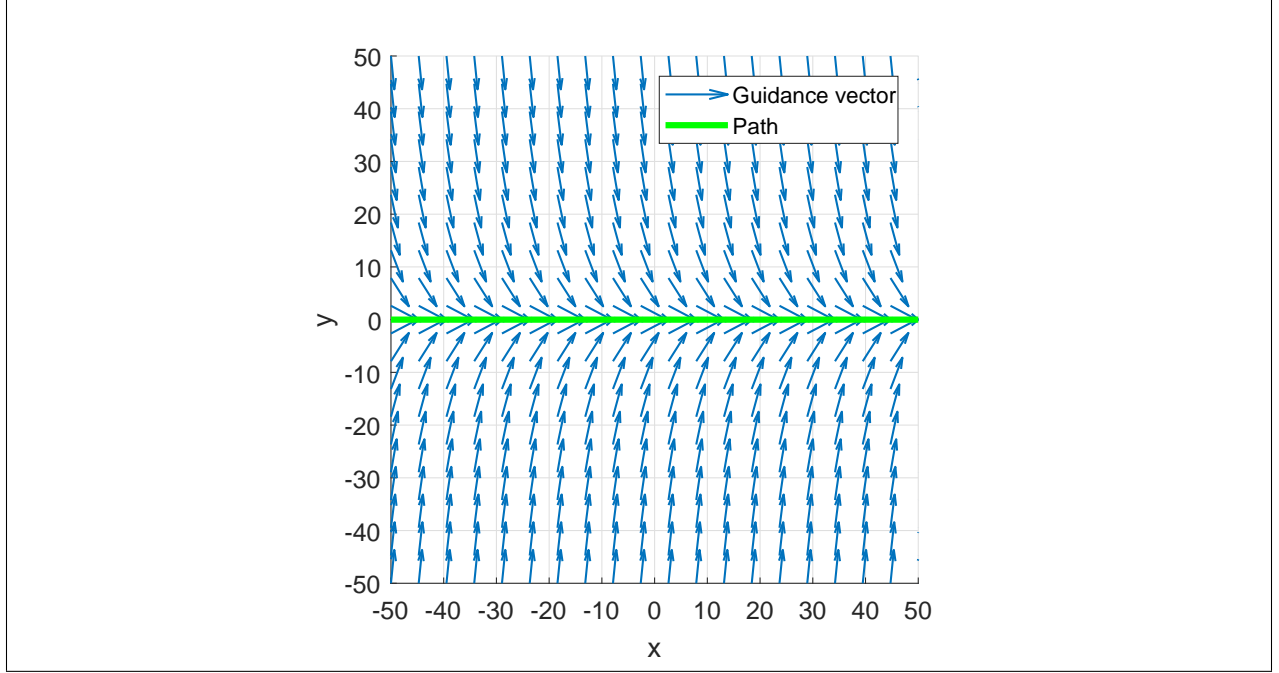


**Fig. 5**

## B. Avoidance

Constructing a repulsive vector field for avoidance using the GVF method starts with constructing a vector field that converges and circulates a circular path. A GVF that converges and circulates a circular path is constructed with the implicit functions of a cylinder of radius  $r$  centered at  $(x_c, y_c)$  and a level plane of constant height  $Z$ , shown in Equations 22 and 23 below.

$$\alpha_1 = (x - x_c)^2 + (y - y_c)^2 - r^2 \quad (22)$$

$$\alpha_2 = z \quad (23)$$

Convergence is determined by the gradient of the potential function 20, which when simplified evaluates to

$$\vec{V}_{conv} = A\vec{B} \quad (24)$$

where

$$A = \frac{-1}{\sqrt{\bar{x}^4 + \bar{y}^4 + 2\bar{x}^2\bar{y}^2 - 2r^2\bar{x}^2 - 2r^2\bar{y}^2 + r^2 + z^2}} \quad (25)$$

and

$$\vec{B} = \begin{bmatrix} 2\bar{x}^3 + 2\bar{x}\bar{y}^2 - 2r^2\bar{x} \\ 2\bar{y}^3 + 2\bar{x}^2\bar{y} - 2r^2\bar{y} \\ z \end{bmatrix} \quad (26)$$

$$\bar{x} = x - x_c \quad (27)$$

$$\bar{y} = y - y_c \quad (28)$$

Circulation is calculated from the cross product of each implicit surface functions gradient, which simplifies to

$$\vec{V}_{circ} = \begin{bmatrix} 2(y - y_c) \\ -2(x - x_c) \\ 0 \end{bmatrix} \quad (29)$$

Guidance for avoiding a circular path with a large radius can be produced by setting the convergence weight  $G = -1$  and circulation weight  $H = 0$ , shown in Figure 6. Note that the vectors are normalized prior to applying decay to ensure the vector field strength is bounded.

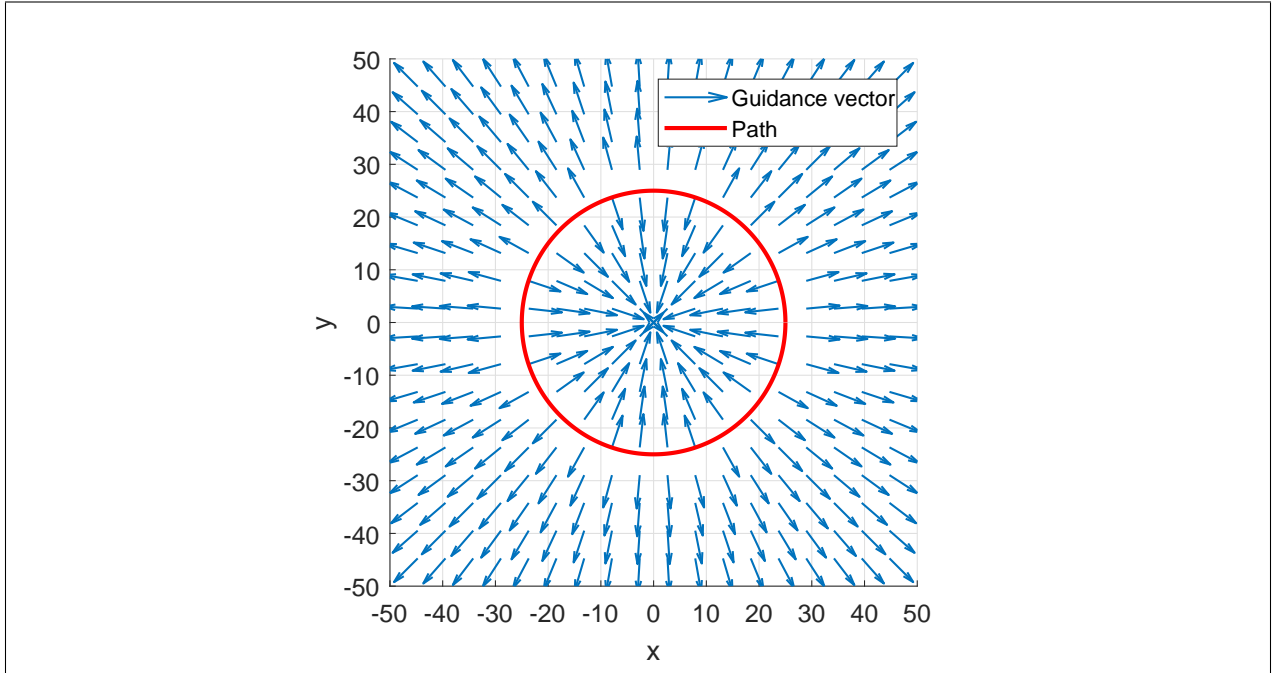


**Fig. 6**

Note that inside of the path, vectors point towards the center of the circle which may produce a trap situation if the UAV ends up inside the radius. To prevent a trap situation inside of the circular path, the radius of the path can be reduced, as shown in Figure 7 where  $r = 0.01$ .



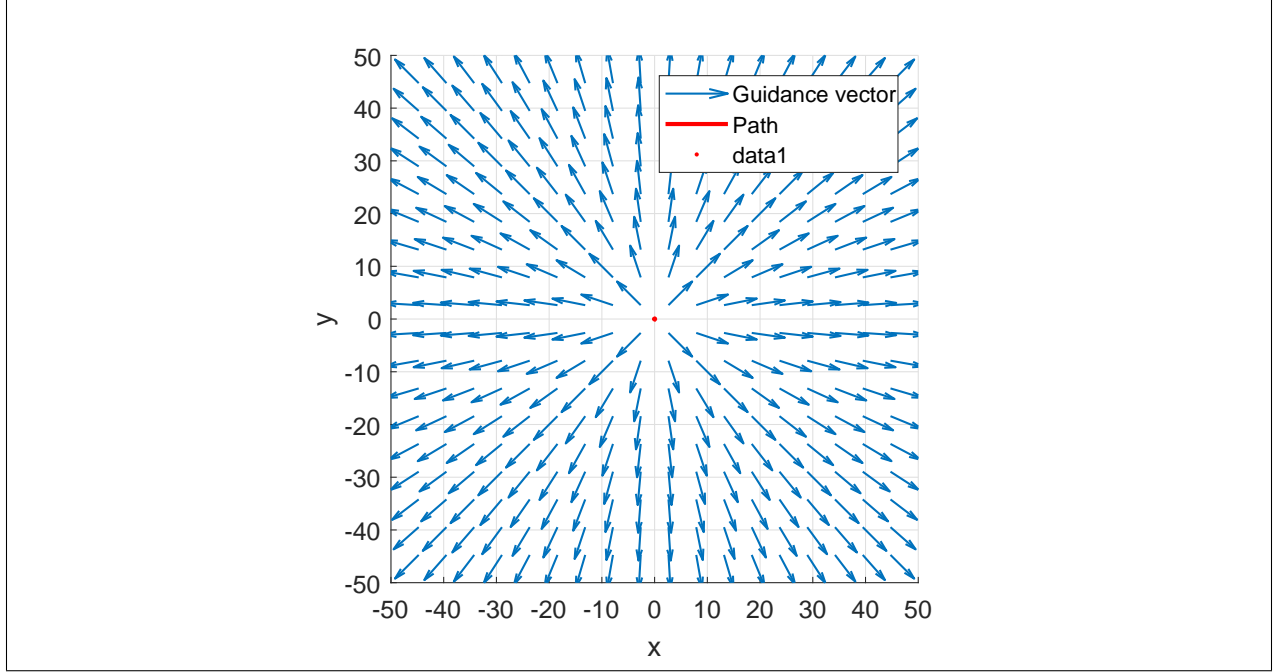


**Fig. 7**

To limit the influence of the repulsive field to a radius  $R$ , a decay function is applied prior to summing with the path following guidance. The decay strength  $P$  is determined in 30, where  $d$  is the euclidean distance, or range, between the UAV and the center of the obstacle, shown in Equation 31. At a distance  $d > R$  the decay strength  $P$  is effectively zero, having virtual no influence on the total guidance. At a distance  $d \leq R$ , the field strength is bounded between  $[0, 2]$ .

$$P = -\tanh\left(\frac{2\pi d}{R} - \pi\right) + 1 \quad (30)$$

$$d = \sqrt{\bar{x}^2 + \bar{y}^2} \quad (31)$$

Applying the decay function with a decay edge radius  $R = 35$  to the GVF shown in figure 7, results in the field shown in Figure 8.

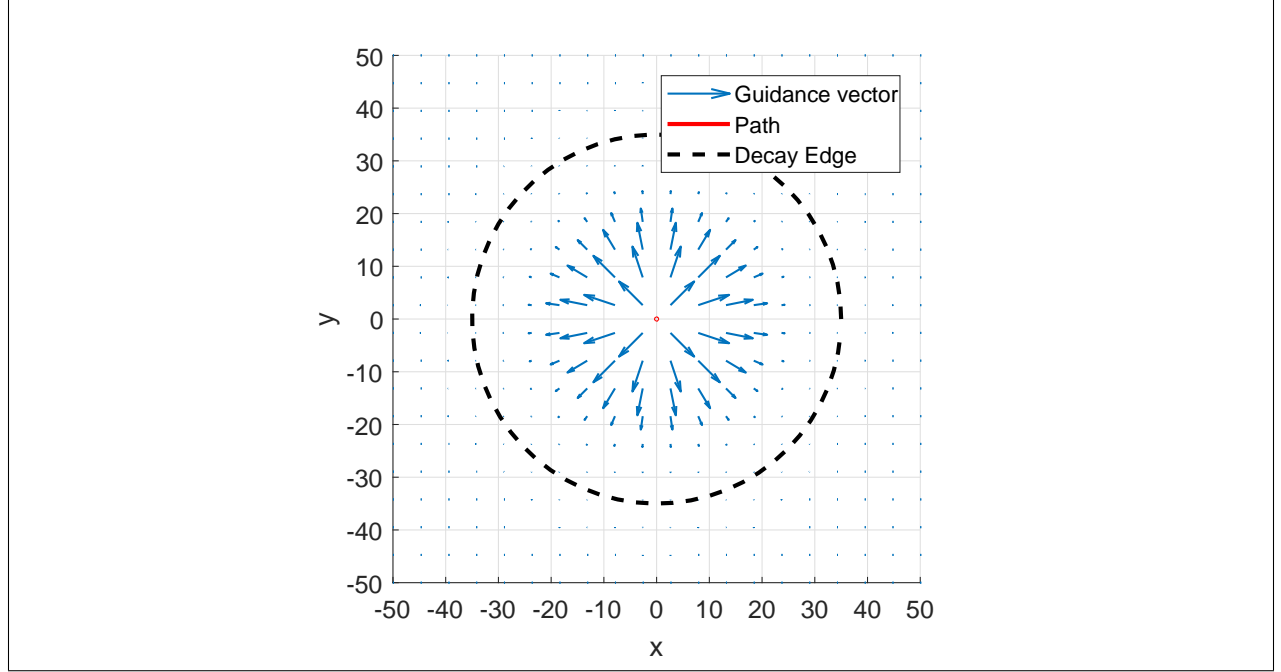


**Fig. 8**

Summing together the path following field with an obstacle centered on the path results in the guidance  $\vec{V}_G$  shown in Figure 9.

$$\vec{V}_g = \vec{V}_{path} + P\vec{V}_{obst} \quad (32)$$

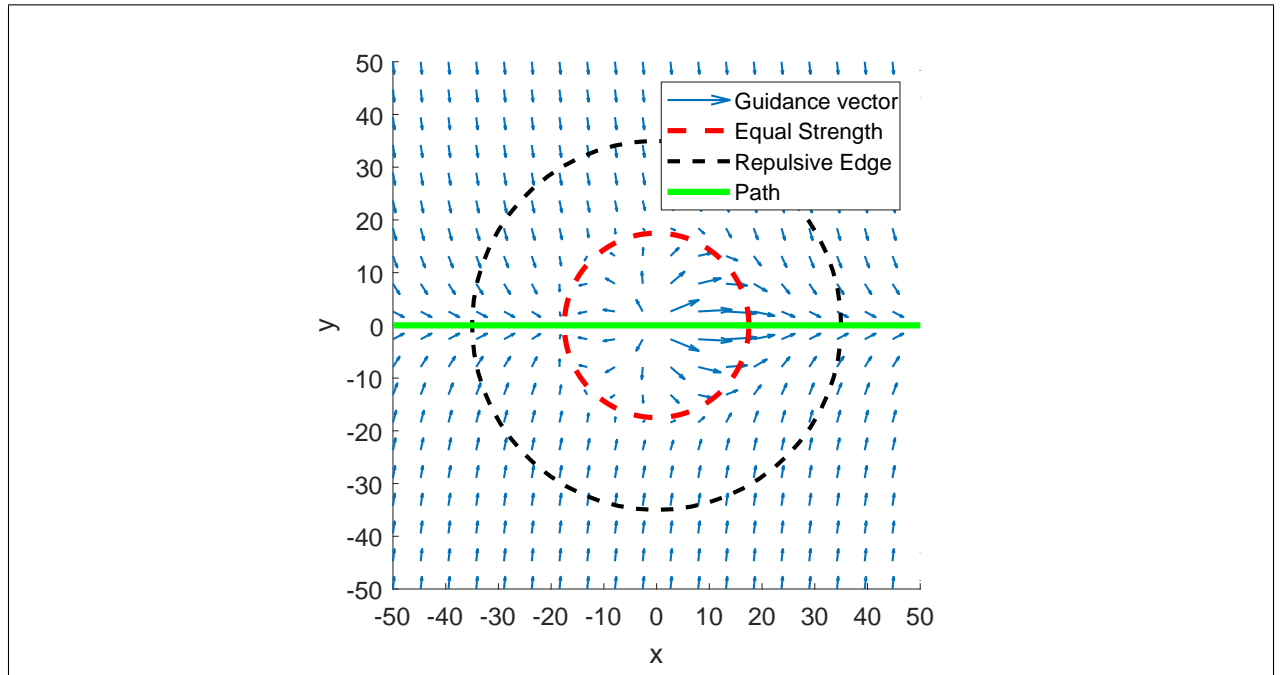


**Fig. 9**

### C. Singularity Detection

$$\|\vec{V}_g\| = 0 \quad (33)$$

Summing GVFs together may lead to small regions where the vector magnitude is near or equal to zero. Singularities are expected to exist where two summed fields have equal strength. The location of the singularities can be found by determining where the magnitude of the resulting guidance is equal to zero.

Plotting the magnitude of the summed field near the obstacle shows a well that descends into several local minimums called singularities, shown in Figure 10.

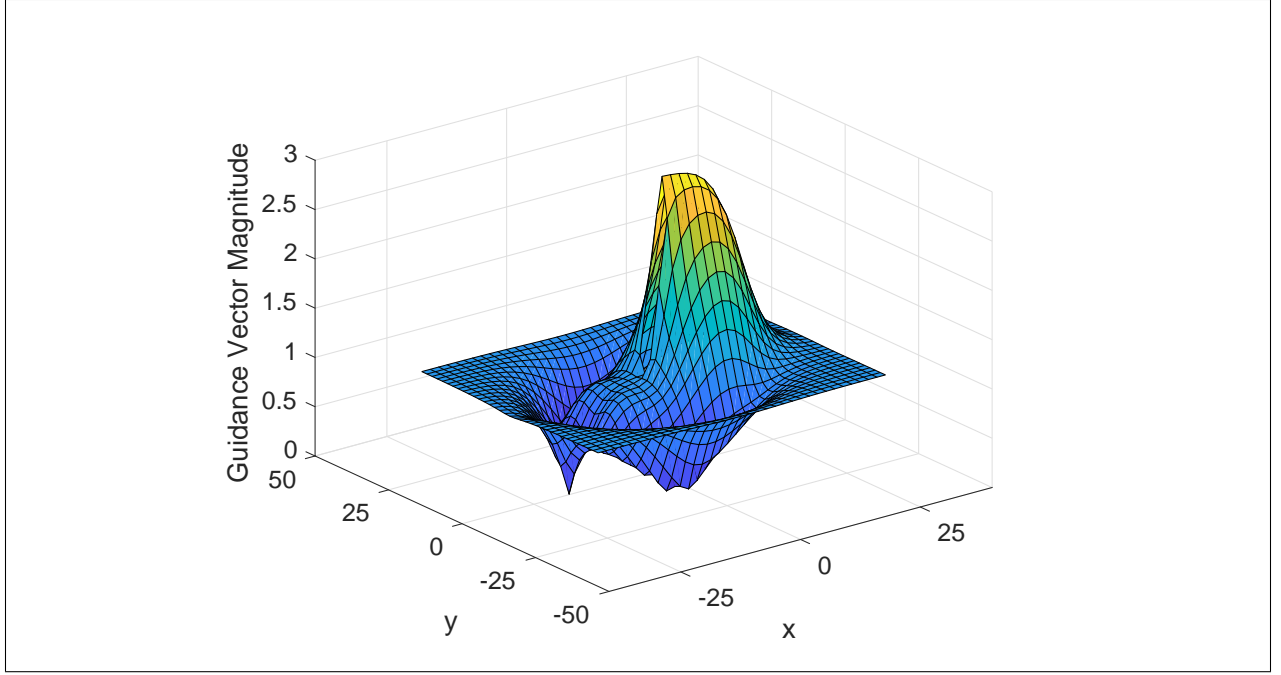


**Fig. 10**

Multiple singularities or near zero guidance regions may exist, so several initial conditions must be evaluated to increase the probability of detection. With the path and obstacle field shown in 9, several initial conditions evenly spaced were evaluated both inside and outside of the equal strength circle. Note how only points left of the obstacle were evaluated since this region is where attractive and repulsive vectors oppose each other, therefore it is where singularities are expected. Both inside and outside initial conditions determine the location of the singularities.

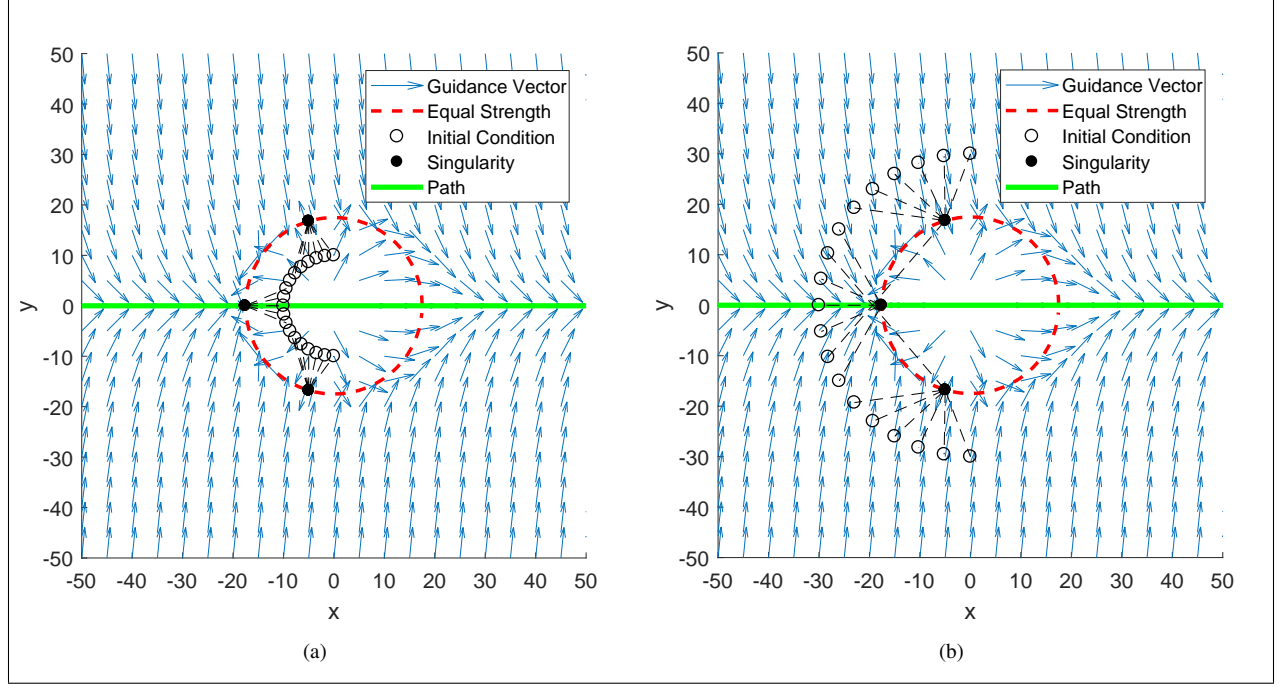


**Fig. 11** GVF converging and circulating circular path

#### D. Flight Envelope

Evaluating a large number of initial conditions to improve the probability of finding singularities may be computationally expensive and may also find singularities the UAV may not encounter. Selecting a reduced set of initial conditions and to determine if the singularities exist where the UAV may fly, a flight envelope is determined for some time horizon  $t_h$ . Consider the UAV depicted in Figure 12 with a turn rate  $\dot{\theta}$  and fixed speed  $u$ .

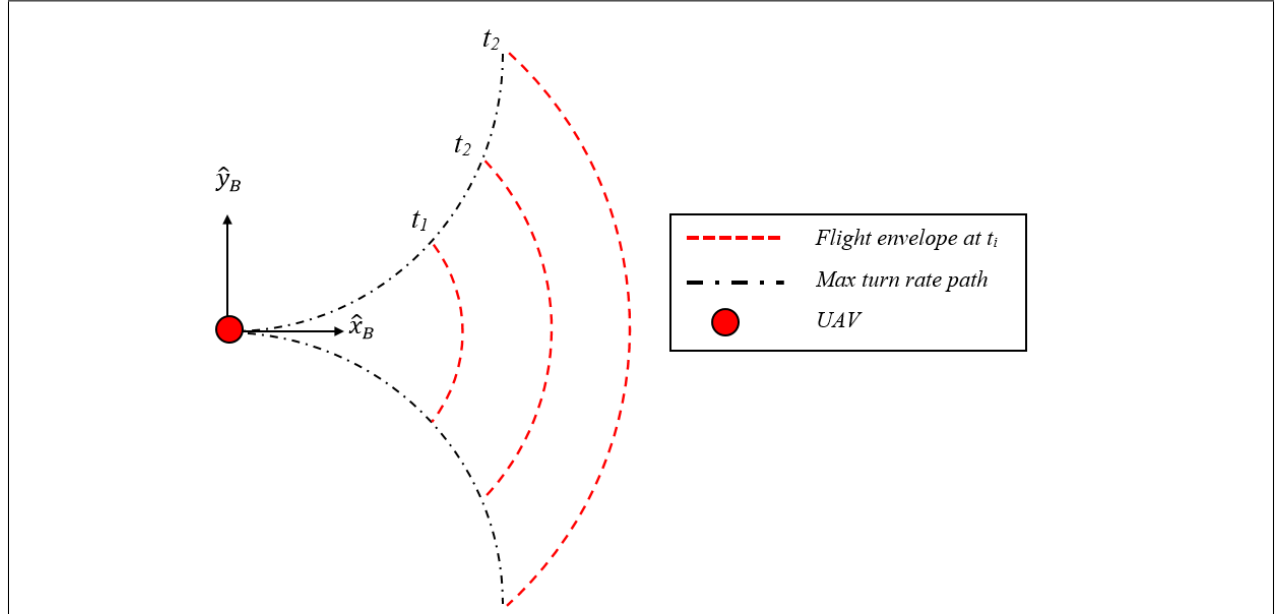


**Fig. 12**

The flight envelope, or positions the UAV, at time  $t_i$  with respect to the body frame is calculated in Equations 34 and 35

$$q_x = \frac{u}{\dot{\theta}} \sin(t_h \dot{\theta}) \quad (34)$$

$$q_y = \frac{u}{\dot{\theta}} (1 - \cos(t_h \dot{\theta})) \quad (35)$$

It is convenient to represent points on the flight envelope in the global inertial frame. The flight envelope points  $(q_x, q_y)$  can be expressed in vector form by finding the angle  $\phi$  with respect to the body frame  $\hat{x}_b$  axis and the vector magnitude  $q$  shown in equations 36 and 37 respectively.

$$\phi = \tan^{-1} \left( \frac{q_y}{q_x} \right) \quad (36)$$

$$q = \sqrt{q_x^2 + q_y^2} \quad (37)$$

$$\vec{Q}_b = \begin{bmatrix} q \cos \phi \\ q \sin \phi \\ 0 \end{bmatrix} \quad (38)$$

To express the flight envelope in the global inertial frame, the position vector of the UAV  $\vec{P}_0$  and  $\theta$  are applied with a rotation matrix  $R$ , shown in Equations 41, 39, and 40 below.

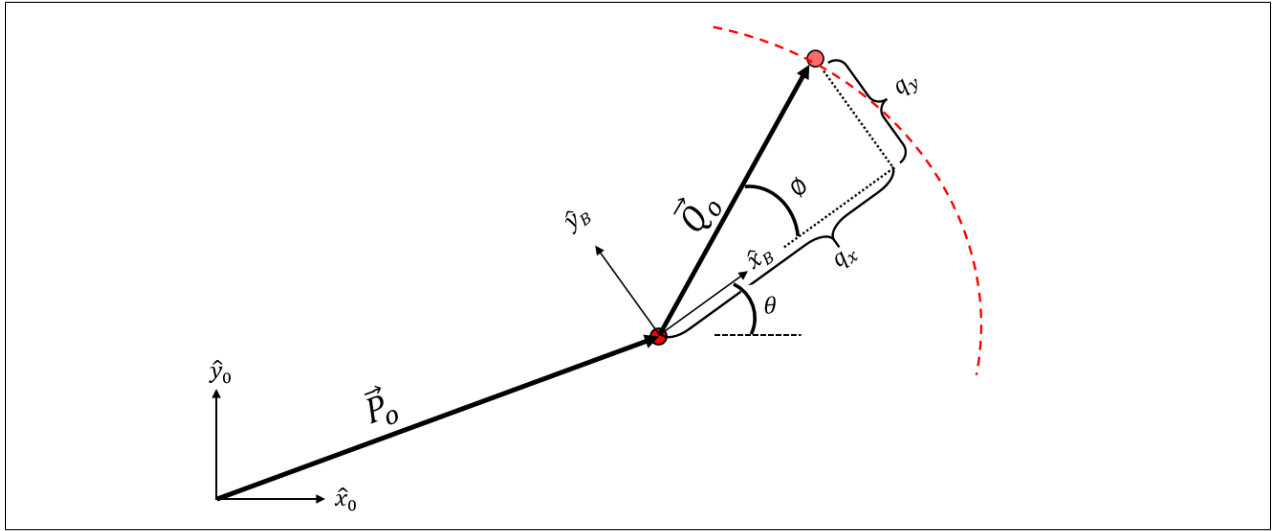


**Fig. 13**

$$\vec{P}_0 = \begin{bmatrix} x & y & 0 \end{bmatrix}^T \quad (39)$$

$$R = \begin{bmatrix} \cos(\theta) & -\sin(\theta) & 0 \\ \sin(\theta) & \cos(\theta) & 0 \\ 0 & 0 & 1 \end{bmatrix} \quad (40)$$

$$\vec{Q}_0 = \vec{P}_0 + R\vec{Q}_b \quad (41)$$

Initial conditions placed on the flight envelope will follow the magnitude gradient of the GVF guidance and locate any singularities it may encounter. When a singularity is found to exist inside or near a flight envelope the field can be modified to counteract it.

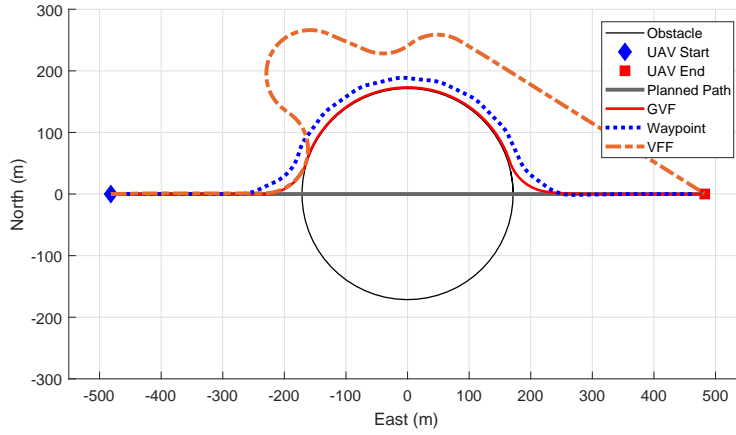


Fig. 14

## IV. Simulations

## V. Conclusion

Method	Cost (-)	RMS Error (m)
Waypoint	16.34	16.75
VFF	34.87	91.65
GVF	13.79	1.65

## Appendix

## Acknowledgments

## References

- [1] Ariyur, K. B., and Fregene, K. O., "Autonomous tracking of a ground vehicle by a UAV," *American Control Conference*, 2008, IEEE, 2008, pp. 669–671.
- [2] Teuliere, C., Eck, L., and Marchand, E., "Chasing a moving target from a flying UAV," *Intelligent Robots and Systems (IROS), 2011 IEEE/RSJ International Conference on*, IEEE, 2011, pp. 4929–4934.
- [3] Oh, H., Kim, S., Shin, H.-S., Tsourdos, A., and White, B., "Coordinated standoff tracking of groups of moving targets using multiple UAVs," *Control & Automation (MED), 2013 21st Mediterranean Conference on*, IEEE, 2013, pp. 969–977. URL <http://ieeexplore.ieee.org/abstract/document/6608839/>.
- [4] Hyondong Oh, Seungkeun Kim, Hyo-sang Shin, and Tsourdos, A., "Coordinated standoff tracking of moving target groups using multiple UAVs," *IEEE Transactions on Aerospace and Electronic Systems*, Vol. 51, No. 2, 2015, pp. 1501–1514. doi:10.1109/TAES.2015.140044, URL <http://ieeexplore.ieee.org/document/7126199/>.
- [5] Ulun, S., and Unel, M., "Coordinated motion of UGVs and a UAV," *Industrial Electronics Society, IECON 2013-39th Annual Conference of the IEEE*, IEEE, 2013, pp. 4079–4084. URL <http://ieeexplore.ieee.org/abstract/document/6699789/>.
- [6] Wilhelm, J., Clem, G., and Eberhart, G., "Direct Entry Minimal Path UAV Loitering Path Planning," *Aerospace*, Vol. 4, No. 2, 2017, p. 23. doi:10.3390/aerospace4020023, URL <http://www.mdpi.com/2226-4310/4/2/23>.

- [7] Khatib, O., "Real-time obstacle avoidance for manipulators and mobile robots," *The international journal of robotics research*, Vol. 5, No. 1, 1986, pp. 90–98. URL <http://journals.sagepub.com/doi/abs/10.1177/027836498600500106>.
- [8] Rimón, E., "Exact Robot Navigation Using Artificial Potential Functions.pdf," , 1992.
- [9] Borenstein, J., and Koren, Y., "Real-time obstacle avoidance for fast mobile robots in cluttered environments," *Robotics and Automation, 1990. Proceedings., 1990 IEEE International Conference on*, IEEE, 1990, pp. 572–577. URL <http://ieeexplore.ieee.org/abstract/document/126042/>.
- [10] Borenstein, J., and Koren, Y., "The vector field histogram-fast obstacle avoidance for mobile robots," *IEEE transactions on robotics and automation*, Vol. 7, No. 3, 1991, pp. 278–288. URL <http://ieeexplore.ieee.org/abstract/document/88137/>.
- [11] Koren, Y., and Borenstein, J., "Potential Field Methods and their inherent limitations for mobile robot navigation.pdf," , 1991. URL <http://ieeexplore.ieee.org/document/131810/>.
- [12] Liu, Y., and Zhao, Y., "A virtual-waypoint based artificial potential field method for UAV path planning," *Guidance, Navigation and Control Conference (CGNCC), 2016 IEEE Chinese*, IEEE, 2016, pp. 949–953. URL <http://ieeexplore.ieee.org/abstract/document/7828913/>.
- [13] Kim, D. H., "Escaping route method for a trap situation in local path planning," *International Journal of Control, Automation and Systems*, Vol. 7, No. 3, 2009, pp. 495–500. doi:10.1007/s12555-009-0320-7, URL <http://link.springer.com/10.1007/s12555-009-0320-7>.
- [14] Goerzen, C., Kong, Z., and Mettler, B., "A Survey of Motion Planning Algorithms from the Perspective of Autonomous UAV Guidance," *Journal of Intelligent and Robotic Systems*, Vol. 57, No. 1-4, 2010, pp. 65–100. doi:10.1007/s10846-009-9383-1, URL <http://link.springer.com/10.1007/s10846-009-9383-1>.
- [15] Lei Tang, Songyi Dian, Gangxu Gu, Kunli Zhou, Suihe Wang, and Xinghuan Feng, "A novel potential field method for obstacle avoidance and path planning of mobile robot," IEEE, 2010, pp. 633–637. doi:10.1109/ICCSIT.2010.5565069, URL <http://ieeexplore.ieee.org/document/5565069/>.
- [16] Li, G., Yamashita, A., Asama, H., and Tamura, Y., "An efficient improved artificial potential field based regression search method for robot path planning," IEEE, 2012, pp. 1227–1232. doi:10.1109/ICMA.2012.6283526, URL <http://ieeexplore.ieee.org/document/6283526/>.
- [17] Sujit, P., Saripalli, S., and Sousa, J. B., "Unmanned Aerial Vehicle Path Following: A Survey and Analysis of Algorithms for Fixed-Wing Unmanned Aerial Vehicles," *IEEE Control Systems*, Vol. 34, No. 1, 2014, pp. 42–59. doi:10.1109/MCS.2013.2287568, URL <http://ieeexplore.ieee.org/document/6712082/>.
- [18] Nelson, D. R., "Cooperative control of miniature air vehicles," 2005. URL <http://scholarsarchive.byu.edu/etd/1095/>.
- [19] Nelson, D. R., Barber, D. B., McLain, T. W., and Beard, R. W., "Vector field path following for small unmanned air vehicles," *American Control Conference, 2006*, IEEE, 2006, pp. 7–pp. URL <http://ieeexplore.ieee.org/abstract/document/1657648/>.
- [20] Nelson, D., Barber, D., McLain, T., and Beard, R., "Vector Field Path Following for Miniature Air Vehicles," *IEEE Transactions on Robotics*, Vol. 23, No. 3, 2007, pp. 519–529. doi:10.1109/TRO.2007.898976, URL <http://ieeexplore.ieee.org/document/4252175/>.
- [21] Frew, E. W., "Cooperative standoff tracking of uncertain moving targets using active robot networks," *Robotics and Automation, 2007 IEEE International Conference on*, IEEE, 2007, pp. 3277–3282. URL <http://ieeexplore.ieee.org/abstract/document/4209596/>.
- [22] Miao, Z., Thakur, D., Erwin, R. S., Pierre, J., Wang, Y., and Fierro, R., "Orthogonal vector field-based control for a multi-robot system circumnavigating a moving target in 3D," *Decision and Control (CDC), 2016 IEEE 55th Conference on*, IEEE, 2016, pp. 6004–6009. URL <http://ieeexplore.ieee.org/abstract/document/7799191/>.
- [23] Griffiths, S., "Vector Field Approach for Curved Path Following for Miniature Aerial Vehicles," *American Institute of Aeronautics and Astronautics*, 2006. doi:10.2514/6.2006-6467, URL <http://arc.aiaa.org/doi/10.2514/6.2006-6467>.
- [24] Goncalves, V. M., Pimenta, L. C. A., Maia, C. A., and Pereira, G. A. S., "Artificial vector fields for robot convergence and circulation of time-varying curves in n-dimensional spaces," IEEE, 2009, pp. 2012–2017. doi:10.1109/ACC.2009.5160350, URL <http://ieeexplore.ieee.org/document/5160350/>.

- [25] Gonçalves, V. M., Pimenta, L. C., Maia, C. A., Pereira, G. A., Dutra, B. C., Michael, N., Fink, J., and Kumar, V., "Circulation of curves using vector fields: actual robot experiments in 2D and 3D workspaces," *Robotics and Automation (ICRA), 2010 IEEE International Conference on*, IEEE, 2010, pp. 1136–1141.
- [26] Gonçalves, V. M., Pimenta, L. C., Maia, C. A., Dutra, B. C., and Pereira, G. A., "Vector fields for robot navigation along time-varying curves in  $n$ -dimensions," *IEEE Transactions on Robotics*, Vol. 26, No. 4, 2010, pp. 647–659. URL <http://ieeexplore.ieee.org/abstract/document/5504176/>.
- [27] Gerlach, A. R., *Autonomous Path-Following by Approximate Inverse Dynamics and Vector Field Prediction*, University of Cincinnati, 2014. URL <http://search.proquest.com/openview/432d738d856bf0a9b46acea1b1ee08f/1?pq-origsite=gscholar&cbl=18750&diss=y>.
- [28] Jung, W., Lim, S., Lee, D., and Bang, H., "Unmanned Aircraft Vector Field Path Following with Arrival Angle Control," *Journal of Intelligent & Robotic Systems*, Vol. 84, No. 1-4, 2016, pp. 311–325. doi:10.1007/s10846-016-0332-5, URL <http://link.springer.com/10.1007/s10846-016-0332-5>.
- [29] Panagou, D., "Motion planning and collision avoidance using navigation vector fields," *Robotics and Automation (ICRA), 2014 IEEE International Conference on*, IEEE, 2014, pp. 2513–2518. URL <http://ieeexplore.ieee.org/abstract/document/6907210/>.